Vibrational Approach to the Dynamics of an α-Helix

RONALD M. LEVY and MARTIN KARPLUS, *Department of Chemistry, Harvard University, Cambridge, Massachusetts 02138*

Synopsis

The dynamics of a finite α-helix have been studied in the harmonic approximation by a vibrational analysis of the atomic motions about their equilibrium positions. The system was represented by an empirical potential energy function, and all degrees of freedom (bond lengths, bond angles, and torsional angles) were allowed to vary. The complete results were compared with a more restrictive model in which the peptide dihedral angle was kept rigid; also, a model potential excluding hydrogen bonds was examined. Thermal fluctuations in the backbone dihedral angles ϕ and ψ are 12° to 15°. The fluctuations of adjacent dihedral angles are highly correlated, and the correlation pattern is affected by the flexibility of the peptide dihedral angle. Time-dependent autocorrelations in the motion of ϕ and ψ appear to decay due to dephasing in less than 1 psec, while the motions of the carbonyl oxygen and amide hydrogens out of the peptide plane are more harmonic. Length fluctuations have been evaluated and exhibit a strong end effect; tha calculated elastic modulus is in agreement with other values. Rigid and adiabatic total energy surfaces corresponding to dihedral angle rotations in the middle of the helix have been obtained and compared with the quadratic approximation to those surfaces. The magnitudes and correlations between the fluctuations obtained by averaging over the adiabatic energy surface most closely resemble the vibrational results. Of particular interest is the fact that hydrogen bonds play a relatively small role in the local dihedral angle fluctuations, though the hydrogen bonds are important in the energy of overall length changes.

INTRODUCTION

A knowledge of the internal mobility of globular and fibrous proteins is fundamental to an understanding of their properties. Much recent experimental[1-9] and theoretical[10-13] work has been devoted to this subject. For globular proteins, internal motions have been implicated in such processes as enzyme catalysis,[6] hemoglobin cooperativity,[12] and immunoglobin action.[13] Studies of mobility in fibrous proteins[7,8,10,11] have served to establish relationships between their mechanical properties and underlying structure. Since the α-helix is an important structural element of many proteins, an understanding of helix dynamics, which is of intrinsic interest, can also serve as the basis for interpreting the internal motions of the more complicated systems.

Among the theoretical approaches to the internal dynamics of a polypeptide chain or protein, there are two of particular importance: the method of "molecular dynamics" and the method of "harmonic analysis." In the molecular dynamics approach, the classical equations of motion for

Biopolymers, Vol. 18, 2465–2495 (1979)

0006-3525/79/0018-2465$01.00

the atoms are solved simultaneously and detailed information is extracted by analyzing the resultant trajectories. Since the full interatomic potential is employed to obtain the forces on the atoms, it is possible to treat large-scale anharmonic motions. The method has recently been applied to the internal dynamics of a globular protein.[9] In highly harmonic systems (e.g., small oscillations of atoms about their equilibrium configuration), the energy is not easily exchanged between the normal modes, and considerable care is required in a molecular dynamics study to avoid biasing the phase space of the trajectories by the choice of initial conditions. For such cases, the harmonic analysis approach to the dynamics is well suited. It neglects the anharmonic contributions to the potential energy and uses the normal modes of the system to obtain the correlation functions and other properties of interest. The fact that the calculations are analytic, given the normal modes, makes harmonic dynamics the method of choice for systems to which it is applicable.

One of the important structural elements of both globular and fibrous proteins is the α-helix. Earlier work on this system includes the measurements of the ir and Raman spectra and their analysis in terms of the normal mode vectors.[14-16] Also, simplified models have been introduced to interpret the low-frequency vibrations and relate them to the phonon dispersion curve for the infinite chain.[17-19] Static correlations of backbone dihedral angle fluctuations have been obtained within the harmonic approximation in the restricted configurational space of the (ϕ,ψ) angles.[10,11] These correlations have been used[10,11] to evaluate geometrical fluctuations and mechanical strengths of sections of the α-helix.

In this paper, we report a harmonic analysis of the dynamic properties of the α-helix. Our approach is to treat a finite chain model α-helix (deca- and hexadecaglycine) and evaluate its energy in the conformational space of all degrees of freedom by use of empirical potential energy functions. Dynamical results were obtained from a complete vibrational analysis of α-helical hexadecaglycine; inclusion of all bond lengths and bond angles, as well as the dihedral angles, results in 252 degrees of freedom. The model system is thus sufficiently complex so that it includes the interaction of a large number of possible internal motions, yet it is sufficiently small so that the normal modes and frequencies can be obtained by diagonalizing the second-derivative potential energy matrix.

An analysis is made of the minimum energy conformation of the constrained helix and of conformations corresponding to uniform compression and extension of the helix generated by concerted changes in all the dihedral angles. Energy surfaces obtained by varying only the dihedral angles are compared with those found when the distorted helix is allowed to reduce some of its strain by relaxing other degrees of freedom. Equilibrium fluctuations in all the internal coordinates (bond length, bond angles, and dihedral angles) are obtained in the harmonic approximation from a normal mode analysis of the helix. Correlations among these fluctuations are examined and related to the tendency of the system to preserve α-helical

structure. Both time-independent and time-dependent correlation functions for fluctuations in the dihedral angles of the helix are obtained in the harmonic approximation to the dynamics. To test the adequacy of the harmonic results, the full potential energy surface is examined and compared with the quadratic approximation to it.

METHODOLOGY

The model systems considered are α-helical deca- and hexadecaglycine with the amino and carboxyl ends blocked by CH_3CO and $NHCH_3$ groups, respectively. Including these end groups, decaglycine contains 8 helical hydrogen bonds (residue i bonded to residue $i + 4$); for hexadecaglycine, there are 14 such hydrogen bonds. All atoms are treated explicitly except for those in the CH_2 and CH_3 groups; these are represented as extended atoms.[20,21]

The empirical potential energy function is written as a sum of terms corresponding to bonds, bond angles, torsional angles, van der Waals interactions, electrostatic interactions, and hydrogen bonds.[20,21] The resulting expression is

$$E(\mathbf{R}) = \frac{1}{2}\sum_{\text{bond}} K_b(b - b_0)^2 + \frac{1}{2}\sum_{\substack{\text{bond}\\\text{angles}}} K_\theta(\theta - \theta_0)^2 + \frac{1}{2}\sum_{\substack{\text{torsional}\\\text{angles}}} K_\phi[1 + \cos(n\phi - \delta)] + \sum_{\substack{\text{nonbonded}\\\text{pairs}}}\left(\frac{A}{r^{12}} - \frac{C}{r^6} + \frac{q_1q_2}{Dr}\right) + \sum_{\substack{\text{hydrogen}\\\text{bonds}}}\left(\frac{A'}{r^{12}} - \frac{C'}{r^{10}}\right) \quad (1)$$

The energy as given by Eq. (1) is a function of the Cartesian coordinate set (**R**) specifying the positions of all the atoms, but the calculation is carried out by evaluating the coordinates for bonds b, bond angles θ, dihedral angles ϕ, and interparticle distances r for any given geometry **R** and determining the contributions using the force constant parameters K_b, K_θ, K_ϕ, Lennard-Jones parameters A and C, atomic charges q_i, dielectric constant D, hydrogen-bond parameters A' and C', and geometrical reference values ("zero-values") b_0 θ_0, n, and δ. Most of the parameters have been given previously for the corresponding potential function applied to proteins.[21] Since N–H hydrogens are treated explicitly in the present case, appropriate parameter changes are required. The individual charges and van der Waals radii are −0.200, 1.55 Å for N and 0.120, 1.47 Å for H; the well depth of the hydrogen-bond function is −3.86 kcal/mol at an O,H atomic separation of 1.89 Å. The hydrogen-bond function [last term in Eq. (1)] was summed over all pairs of hydrogen-bonded O,H atoms and replaced the van der Waals interaction between these directly hydrogen-bonded O,H pairs. The NH bond stretching force constant employed was 405 kcal/mol Å^2, and the in-plane angle bending force constants involving the amide hydrogen atoms

were 31.4 and 38.2 kcal/mol rad^2 for the C^α—N—H and H—N—C′ angles, respectively. Also, it is to be noted that the motion of the amide hydrogen and carbonyl oxygen atoms out of the plane of the peptide bond are described by improper torsional angles.[21] The angle that describes the improper torsion of the amide hydrogens $\chi(C',N,H,C^\alpha)$ is defined as the angle between the planes specified by C′,N,H and N,H,C^α; a corresponding definition is used to describe the improper torsion of the carbonyl oxygen $\chi(C^\alpha,C',O,N)$. The associated force constants are K_χ(N—H) = 0.7 kcal/mol and K_χ(C—O) = 5.75 kcal/mol. Model studies were made in which some of the important parameters of the potential function were varied. One of these concerns the torsion about the peptide dihedral angle ω. For most of the calculations, a low value of K_ω = 2.9 kcal/mol was used and comparisons were made with the commonly employed K_ω = 7 kcal/mol, as well as with an essentially rigid peptide torsional potential, K_ω = 100 kcal/mol.

Since hydrogen bonds are expected to play an important role in the α-helix, the potential function used for them was examined in some detail. Figure 1 shows the total hydrogen-bond energy of a C=O fragment interacting with an N–H fragment as a function of geometry; the O···H distance and N—H···O and H···O=C angle dependencies are given. The shape of

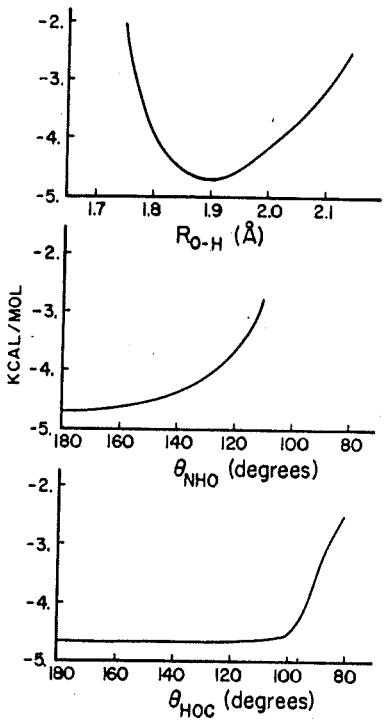

Fig. 1. Total hydrogen-bond energy of the CO, NH fragments; the total hydrogen-bond energy is the sum of hydrogen bond, nonbonded and electrostatic interactions of CO with NH.

the potential is similar to that reported by Hagler and Lifson[22] for the amide hydrogen bond. Since no explicit angular dependence is included in the potential function [Eq. (1)], the observed variation of the hydrogen-bond energy with angle results from the nonbonded and electrostatic two-body interactions of the atoms of the N—H, C=O fragment. The effect of eliminating the hydrogen bonds from the helix was studied by removing the (10,12) term from Eq. (1); the remaining interactions (nonbonded and electrostatic) between the fragments create a potential that is mainly repulsive, with a very shallow van der Waals minimum (0.1 kcal/mol) at an O···H distance of 2.55 Å.

By employing transformations between Cartesian and internal coordinates, the first and second derivatives of Eq. (1) can be obtained analytically. Energy minimization was achieved with first derivatives using steepest descent and conjugate gradient methods[23] and with second derivatives using the Newton-Raphson method[24]; for the latter, the second-derivative matrix was diagonalized in the standard fashion.[24] A cycle of 50 steepest descents followed by 5 Newton-Raphson for hexadecaglycine required about 3.5 min on the IBM 360/91.

Rigid-geometry contour maps corresponding to uniform compression and elongation of the helix were generated by changing the dihedral angles ϕ and ψ together in 1° increments; a uniform increase in ϕ and ψ of 1° for all of the residues in decaglycine lengthens the helix by about 0.3 Å. Uniform changes in the dihedral angles of the helix lead to short nonbonded contacts that are easily relieved by small changes in helical structure. To incorporate such relaxation effects, adiabatic geometry contours were constructed by constrained energy minimization.[21] A cycle of 200 steepest descent minimization steps was performed for each of the rigid-geometry conformations in the presence of a constraining potential applied to the first and last C^α atoms; the latter fixed the overall length of the relaxed helix to be the same as the corresponding rigid conformation but allowed for readjustment of dihedral angles, as well as bond lengths and bond angles.

The starting point for a vibrational analysis and a harmonic dynamics treatment of the α-helix is the stable equilibrium conformation. For the minimization of decaglycine in the complete conformational space 75 steepest-descent steps followed by five cycles of 5 Newton-Raphson steps each were required to eliminate the negative eigenvalues corresponding to local maxima that appeared in intermediate steps. Each successive Newton-Raphson cycle included progressively lower frequency eigenvectors in the search procedure. At the conformational minimum of decaglycine, the final rms derivative was 0.0008 kcal/mol Å and the lowest nonzero frequency was 14.16 cm^{-1}.

Given the stable local minimum geometry, the normal-mode frequencies are obtained[25] from the secular equation

$$|\mathbf{F} - \omega^2\mathbf{T}| = 0 \tag{2}$$

where $\mathbf{F}$ is the Cartesian second-derivative potential energy matrix (F_{ij} =

$\partial^2 V/\partial x_i \partial x_j$) and $\mathbf{T}$ is the Cartesian kinetic energy matrix ($T_{ij} = \delta_{ij} m_i$, with m_i the mass of atom i). Of the $3N$ eigenvalues of Eq. (2), $3N - 6$ corresponded to normal frequencies, $\nu_i (\nu_i = \omega_i/2\pi)$, with associated normal-mode eigenvectors, Q_i; the components of Q_i give relative amplitudes of the contributing atomic displacements expressed in terms of mass-scaled Cartesian coordinates.

Quantities of primary interest in a dynamical analysis are the correlation functions[26] of the form $\langle \Delta A(t) \Delta A(t + \tau) \rangle$, where $\Delta A(t)$ is the fluctuation at time t of the variable A from its mean value $\langle A \rangle$, and the brackets indicate an ensemble average. For an equilibrium system, the correlation function is independent of t and is often written $\langle \Delta A(0) \Delta A(\tau) \rangle$. The equal-time correlation function, $\langle [\Delta A(0)]^2 \rangle$, is the mean-square thermal fluctuation of A from its equilibrium value, and $\langle \Delta A(0) \Delta A(\tau) \rangle$ describes the time decay of this fluctuation. In the harmonic approximation to the system dynamics, the position and velocity correlation functions can be evaluated from the set of normal coordinates $\{Q_i\}$ and normal angular velocities $\{\omega_i\}$ found from Eq. (2). The correlation between any two normal coordinates, Q_i and Q_j, is given by[27]

$$\langle Q_i(t_1) Q_j(t_2) \rangle = \delta_{ij} \frac{KT}{\omega_i^2} \cos \omega_i (t_1 - t_2) \tag{3}$$

where K is the Boltzmann constant and T is the absolute temperature. Writing the displacement of an internal coordinate A from the mean value as a sum of normal coordinate displacements,

$$\Delta A(t) = \sum_{i=1}^{3N-6} \alpha_i Q_i(t) \tag{4}$$

where α_i is the component of Q_i in the direction of A, the position correlation function is found to be

$$\langle \Delta A(0) \Delta A(t) \rangle = KT \sum_{i=1}^{3N-6} \frac{\alpha_i^2}{\omega_i^2} \cos \omega_i t \tag{5}$$

The velocity correlation function can be obtained from the equation

$$\langle \Delta \dot{A}(0) \Delta \dot{A}(t) \rangle = -\frac{d^2}{dt^2} (\langle \Delta A(0) \Delta A(t) \rangle) = KT \sum_{i=1}^{3N-6} \alpha_i^2 \cos \omega_i t \tag{6}$$

where the first equality can be shown to be valid for an equilibrium system.[28]

To obtain information about the limitations of the harmonic dynamics analysis, the potential energy surface about the neighborhood of the α-helical minimum energy conformation was examined and a comparison was made between the exact surface and the quadratic approximation to it. Both rigid and adiabatic (ϕ,ψ) dihedral-angle surfaces were used in this comparison. The exact rigid (ϕ,ψ) surface was constructed by rotating the two angles ϕ_6 and ψ_6 of decaglycine away from their equilibrium values at 4° intervals up to ±20° without any energy minimization. This surface

would govern the motion of the helix if all degrees of freedom except ϕ_6, ψ_6 were held fixed. To include relaxation effects, the corresponding exact adiabatic surface was constructed. The dihedral angles ϕ_6 and ψ_6 were again rotated away from their equilibrium values in 4° increments up to ±20°. However, after each 4° change in a dihedral angle, energy minimization of the helix was performed with a combination of conjugate gradient and Newton-Raphson steps while ϕ_6 and ψ_6 were held at the given value by a large constraining potential. The resulting surface would govern the motion of ϕ_6 and ψ_6 if all other degrees of freedom were able to relax adiabatically in response to fluctuations in ϕ_6 and ψ_6. The rigid and adiabatic results thus represent limiting surfaces; that is, the portion of the full multidimensional potential surface which governs the motion of ϕ_6 and ψ_6 is expected to be more flexible than the rigid geometry surface yet somewhat less flexible than the adiabatic surface. Calculation of the rigid surface is very rapid; to generate the complete adiabatic surface, approximately 1 hr of IBM 360-91 computer time was required.

To obtain the harmonic approximations to the exact rigid and adiabatic surfaces, the Cartesian second-derivative matrix $\mathbf{F}$ (Eq. 2) was expressed in internal coordinates. This simplifies the calculation and separates out the overall translation and rotations that are introduced when the (ϕ_6,ψ_6) dihedral angle pair is varied. The internal coordinate quadratic potential energy matrix $\mathbf{F}$ was obtained from the relation[25]

$$\mathbf{F} = \mathbf{G}^{-1} \cdot \mathbf{L} \cdot \mathbf{\Lambda} \cdot \mathbf{L}^{+} \cdot \mathbf{G}^{-1} \tag{7}$$

where $\mathbf{G}^{-1}$ is the kinetic energy matrix

$$G_{ij}^{-1} = \sum_k m_k \frac{\partial x_k}{\partial S_i} \frac{\partial x_k}{\partial S_j}$$

with S_i a given internal coordinate. $\mathbf{L}$ is the matrix whose columns are the internal coordinate amplitudes contributing to the normal modes, and $\mathbf{\Lambda}$ is the diagonal matrix of normal mode frequencies. Each point on a surface corresponds to a vector $\mathbf{R}$, whose components are the values of the internal coordinates. The quadratic approximation to the empirical potential energy at $\mathbf{R}$ is then

$$2V = \mathbf{R}^{+}\mathbf{F}\mathbf{R} \tag{8}$$

For the rigid surface, $\mathbf{R}$ is the two-component vector (ϕ_6,ψ_6); for the adiabatic surface, all $3N - 6$ internal coordinates are involved.

As a further test of the harmonic surfaces, equal-time correlation functions were estimated from them by Boltzmann averaging; that is, for the correlation function of the fluctuation ΔA and ΔB $(A,B = \phi_6,\psi_6)$, the relation

$$\langle \Delta A(0) \Delta B(0) \rangle \cong \frac{\sum_{\Delta A,\Delta B} \Delta A \Delta B \exp[-E(\Delta A,\Delta B)/KT]}{\sum_{\Delta A,\Delta B} \exp[-E(\Delta A,\Delta B)]/KT} \tag{9}$$

was used, where ΔA and ΔB are summed over the calculated range ($\pm 20°$). The correlation function estimates for the various surfaces are obtained by using the appropriate energy function (rigid total, rigid harmonic, adiabatic total, adiabatic harmonic) when evaluating Eq. (9). The $\pm 20°$ limit is satisfactory for the rigid surface, because at these extremes the energy is already $10KT$ above the minimum. This is not true for the adiabatic surface, but the expense involved in sampling a larger portion of that surface did not appear justified.

RESULTS

In this section, we present and discuss the calculations concerned with the helix potential surface and the resulting dynamics.

Potential Surface for Helix Extension and Compression

We examine the potential surface for extension and compression of the entire helix and compare the results obtained in the rigid and adiabatic approximations. To begin, we consider a regular right-handed decaglycine helix with standard geometric parameters and determine how much the energy-minimized structure differs from the initial regular geometry. The standard bond lengths and bond angles are somewhat arbitrary but reasonable (Table I); the three dihedral angles were chosen equal to $\phi = -57°$, $\psi = -47°$, $\omega = 180°$, in keeping with the IUPAC suggested values,[29] although for decaglycine, the present empirical parameters yield $\phi = -58°$, $\psi = -48°$, $\omega = 180°$ as the energy minimum for the regular α-helix. Gō et al.[30] calculated the energy minimum of the regular polyglycine α-helix to be at $\phi = -52°$, $\psi = -53°$ with $\omega = 180°$. The energy-minimized geometry of α-helical decaglycine is compared with the geometry of the regular α-helix in Table I. As commonly found in conformational energy calculations, the deviations in the average values of bond lengths and bond angles from standard values are small, i.e., 0.01 Å or less for bond lengths and 4° or less for bond angles. The final dihedral angles differ somewhat more from the initial values, especially at the ends of the chain, where the variation is as much as 10°. In the interior of the helix, the dihedral angles vary in a well-defined manner, the ϕ and ψ both increasing by $\sim 3°$ and ω decreasing by 12° from the regular helix values. The improper torsional angles for N—H and C=O show that the former is bent significantly out of the C′—N—C^{α} plane, while the latter is only slightly displaced from its plane. All of these alterations combine to yield a shorter helix with a larger cross section and somewhat improved hydrogen bonds. Table II summarizes the geometric properties of the hydrogen bonds of decaglycine in the initial and energy-minimized conformations. It is clear that the hydrogen bonds are significantly shortened (~ 0.16 Å) and the H - - - O—C angle increases by 4°–6° relative to the regular helix.

Rigid and adiabatic geometry results corresponding to "uniform"

TABLE I
Comparison of Initial and Final α-Helix Geometry[a]

Helical Averages	Initial Geometry	Final Geometry	Final Standard Deviation
Bond length			
$N-C^{\alpha}$	1.490	1.500	<0.001
$C^{\alpha}-C'$	1.530	1.541	0.002
$C'-O$	1.215	1.216	<0.001
$C'-N$	1.305	1.311	0.001
$N-H$	0.980	0.979	<0.001
Bond angles			
$C'-N-C^{\alpha}$	123	122	0.18
$N-C^{\alpha}-C'$	110	113	1.17
$C^{\alpha}-C'-N$	116	120	0.52
$C^{\alpha}-C'-O'$	120	119	0.16
$C^{\alpha}-N-H$	120	118	0.05

Final Values of Individual Dihedral Angles	ϕ	ψ	ω	"Improper" NH	"Improper" CO
Gly 1	–	−53	173	178	178
2	−55	−48	169	174	179
3	−55	−43	168	179	179
4	−54	−46	168	176	179
5	−55	−44	167	176	180
6	−54	−45	168	175	180
7	−55	−43	168	175	180
8	−55	−45	168	175	181
9	−58	−37	167	175	186
10	−64	−41	168	172	187
Mean	−56.1	−44.5	168.4	175.5	181
Standard deviation	3.2	4.2	1.7	1.96	3.24

[a] Bond lengths are in Å and angles are in degrees.

stretching and compression of the helix from the equilibrium length ($\Delta l = 0$) are shown in Figs. 2(a) and 2(b), respectively; the values were obtained as described above. The total energy curve in the rigid geometry map has its minimum at ($\phi = -58°, \psi = -48°$) and increases steeply on both sides. The nonbonded and hydrogen-bond contributions to the energy variation are seen to be similar, though the former is somewhat less steep and has its minimum at a point about 0.03 Å shorter than the latter. Thus the main contribution to the increased rigid geometry conformational energy as the helix is compressed arises from the repulsive portion of the hydrogen-bonding 10–12 potential [Eq. (1)]. As the helix is stretched above its optimal length, the nonbonded repulsions increase rapidly, and the stabilizing contribution of the hydrogen bonds is lost. The adiabatic geometry results shown in Fig. 2(b) are strikingly different from the rigid-geometry calculation. In particular, there is a strong asymmetry in the energy contour in that it is much easier to compress the helix than stretch it. The repulsive

TABLE II
Comparison of Initial and Final Hydrogen-Bond Geometry

	Number of Hydrogen Bond[a]							
	1:5	2:6	3:7	4:8	5:9	6:10	7:$NHCH_3$	CH_3CO:4
$R_{O\cdots H}$ (Å)								
Initial	2.053	2.053	2.053	2.053	2.053	2.053	2.053	2.104
Final	1.886	1.887	1.886	1.888	1.887	1.888	1.893	1.891
θ_{NHO} (deg)								
Initial	164	164	164	164	164	164	164	161
Final	163	163	162	162	161	161	149	164
θ_{HOC} (deg)								
Initial	157	157	157	157	157	157	157	157
Final	164	166	163	165	163	163	161	151

[a] Each hydrogen bond is identified by the two amino acids involved with the first number in the pair corresponding to the CO residue and the second to the NH residue; $NHCH_3$ and CH_3CO corresponds to the carboxy and amino terminal-blocking groups.

contributions from too-close hydrogen-bond contacts that occur during compression in the rigid geometry are easily relaxed by small adjustments of the dihedral angles. These can occur in the adiabatic calculation, since the length constraints are imposed only at the ends of the helix. As the constrained conformations are energy minimized, all of the ϕ and ψ values tend to change. In general, the final values for ϕ are more dependent on the starting helix geometry than are the values of ψ; that is, the final value of ψ averaged over the 10 residues was $-50°$ to $-52°$ regardless of initial geometry, while the average value of ϕ increased progressively as the helix was stretched (e.g., $\langle\phi\rangle = -62°$ for $\Delta l = -2$ Å and $\langle\phi\rangle = -47°$ for $\Delta l = +2$ Å). It is evident from the figure that after relaxation, neither the hydrogen bond nor the van der Waals energy increases when the helix is compressed to $\Delta l = -2$ Å. That the adiabatic total energy curve still displays a shallow minimum at the equilibrium length is due to the electrostatic energy term.

The Young's modulus of elasticity ϵ of a polymer chain can be obtained directly from the change in energy with chain length,[31,32] that is,

$$\epsilon = (\Delta E) l_0 / A (\Delta l)^2 \tag{10}$$

where ΔE is the change in energy due to a change in length Δl, and l_0 and A are the length and cross-sectional area of the chain; the cross-sectional area of the helix is 5.15×10^1 Å^2.[11] From the present calculations, the modulus of elasticity is estimated to be between 1.68×10^{11} dyn/cm^2 (adiabatic energy curve) and 4.8×10^{11} dyn/cm^2 (rigid energy curve). These estimates are close to previous calculations ($2.3–7.2 \times 10^{11}$ dyn/cm^2) based on equilibrium length fluctuations by Suezaki and Gō[11] and Itoh and Shimanouchi[16] but are about an order of magnitude greater than measurements based on macroscopic extensions.[33] A recent determination[34] of

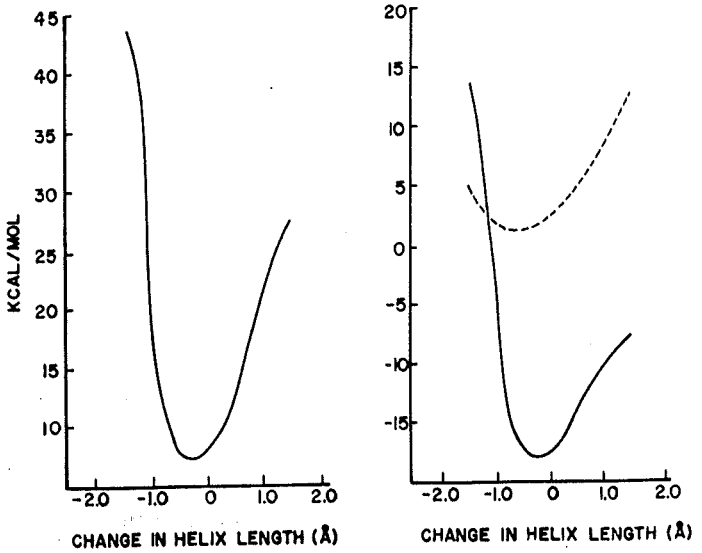

(a)

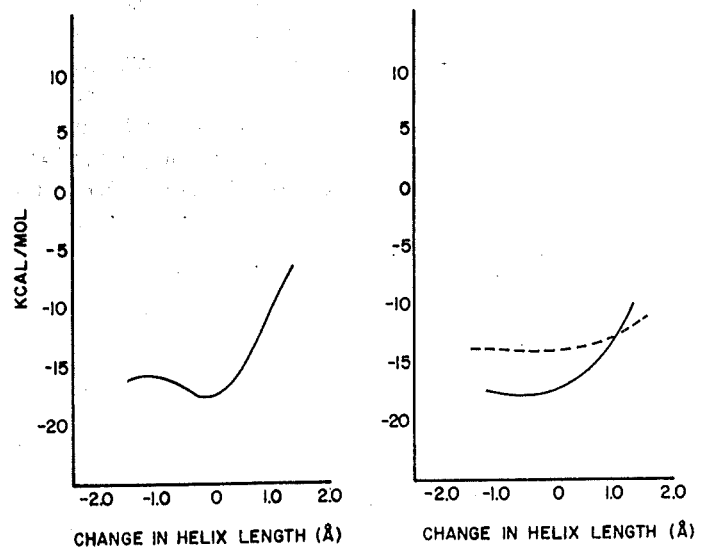

(b)

Fig. 2. Change in energy with stretch and compression of the helix. (a) Left-hand figure gives the change in total energy with rigid deformation of the helix, and the right-hand side gives component change in hydrogen-bond energy, (—) and change in van der Waals energy (- - -). (b) Same except for adiabatic deformation.

the elastic modulus of collagen by laser Brillouin scattering yielded values of 1.5–2.0 × 10^{11} dyn/cm^2, in much closer agreement with the calculations. It was suggested that inhomogeneous strain can account for the small values of elastic moduli obtained from macroscopic extensions.

Harmonic Dynamics of a Helix

Some information about the flexibility of a helix has been obtained from the calculated energy contours described above. A more complete understanding of the dynamic properties requires an examination of the magnitudes, correlations, and time dependencies of the significant geometric variables. This part of the paper provides the results of a dynamical analysis of the helix in the harmonic approximation.

Vibrational Spectrum

Since the dynamical results reported below are based on the harmonic approximation, they reflect the vibrational frequencies and normal modes of the helix. The ir spectra and normal-mode calculations for helical polyglycine II and α-helical polyalanine have been reported previously.[15,16,35,36] The calculated ir spectrum between 200 and 1800 cm^{-1} obtained with the parameters used in this work is shown in Fig. 3. The relative intensities were taken to be proportional to the square of the molecular dipole derivatives with respect to the normal coordinates; the dipole derivatives were obtained from monopoles assigned to each of the atoms.[21] Intense higher-frequency absorptions correspond to the essentially localized motions of the peptide group atoms; in addition, there are the lower-frequency modes that involve larger parts of the α-helix and contribute most importantly to its elastic properties. In a 10-residue α-helix, in contrast to an infinite helix, the atoms of a given residue occupy a nearly (but not

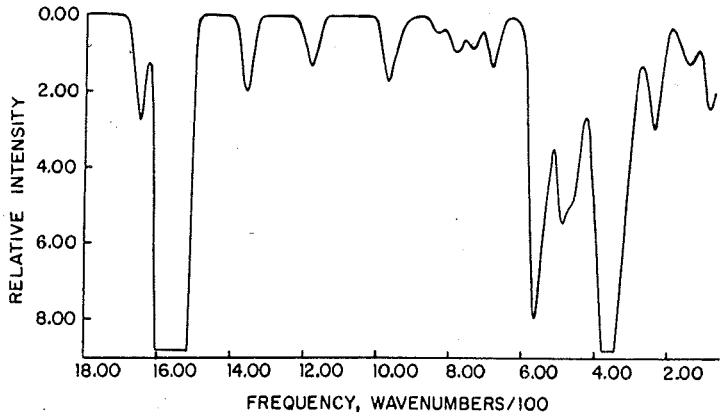

Fig. 3. Calculated vibrational spectrum of decaglycine; absorption at ~3330 cm^{-1} corresponding to the NH stretch modes is not shown.

exactly) equivalent environment with respect to atoms in a neighboring amino acid. The effect of this on any particular local mode is to obtain a band of frequencies instead of a single frequency. For example, the highest frequency mode of the helix, the NH stretch (not shown in Fig. 3), consists of 11 normal modes centered at 3330 cm^{-1} with a bandwidth of 200 cm^{-1}; the experimental value for polyglycine is in the neighborhood of 3300 cm^{-1}. The next set of observed frequencies corresponds to CH stretches of the C^{α} methylene group; these do not appear in the present calculation, because the methylene group is treated as a single extended atom. The intense amide I vibration (CO stretch) appears at 1590–1650 cm^{-1} in the spectrum (experiment 1640–1680 cm^{-1}), while the intense amide II vibration (CN stretch and NH in-plane bend) is at 1530–1560 cm^{-1} (experiment 1500 cm^{-1}). The less intense amide III mode appears in the region of 1370 and 1180 cm^{-1} (experiment 1250 cm^{-1}); the calculated absorption at ~970 cm^{-1} is due to a combination of motions involving the C^{α} carbons; that is, of the $N—C^{\alpha}$ and $C^{\alpha}—C'$ stretches, as well as the $C'—N—C^{\alpha}$ bend (experiment 1015 cm^{-1}). Between 500 and 700 cm^{-1} there appear the amide IV, V, and VI vibrations [CO and NH out-of-plane (improper) torsions]; the experimental range is 490–700 cm^{-1}. The intense absorption at 570 cm^{-1} is due to a combination of these motions. Absorption in the far-ir region is the result of more complicated motions of the helix. The strong absorption at 368 cm^{-1} has contributions from out-of-plane torsional and in-plane bending vibration of the C=O and NH groups; it appears to correspond to the amide VII vibration observed at 360 cm^{-1}. Below 300 cm^{-1}, the infrared absorption is weak. The dominant contributions to these frequency modes are helix deformations which arise from torsional motions of the ϕ,ψ dihedral angles of the helix; they are discussed below.

Magnitude of Fluctuations

Bond-length fluctuations—which arise from localized, high-frequency vibrations—are on the order of 0.02–0.03 Å. The spectral densities of the fluctuations in NH, CO, and NC bond lengths of residue 8 in hexadecaglycine are shown in Table III. That one mode is dominant for the NH bond is due to the near degeneracy of the stretching modes and the lack of complete symmetry in the system studied. The bond-length fluctuations are not sensitive to details of the structure of the α-helix; those at the end of the helix are identical to the ones found in the middle. Furthermore, the magnitude of the fluctuations are accounted for by the numerical value of the bond stretching force constants. Bond angle fluctuations have magnitudes of 3°–5°. As for the bond lengths, the magnitudes of the angular fluctuations are the same throughout the helix. An analysis of the spectral densities shows that a broader range of frequencies contributes to the angular motions (Table III).

Most of the helix flexibility, as well as correlations in fluctuations imposed by nonbonded constraints, involved the dihedral angles. The

TABLE III
Typical Spectral Densities of Bond Length and Bond Angle Fluctuations[a]

Coordinate	Frequency[b] (cm^{-1})	Amplitude ($Å^2 \times 10^4$)	All Frequencies
$\langle[\Delta b(NH)]^2\rangle$	3434	6.24	7.31
	3433	0.08	
$\langle[\Delta b(CO)]^2\rangle$	1597	0.75	4.99
	1592	0.54	
	1608	0.35	
	1609	0.34	
	1605	0.31	
$\langle[\Delta b(NC^\alpha)]^2\rangle$	988	1.56	11.15
	960	1.15	
	972	0.75	
	983	0.74	
	946	0.72	
		$(deg)^2$	$(deg)^2$
$\langle[\Delta\theta(C^\alpha C'O)]^2\rangle$	446	1.17	14.60
	387	1.08	
	409	0.92	
	509	0.82	
	400	0.82	
$\langle[\Delta\theta(NC^\alpha C')]^2\rangle$	188	2.34	26.43
	163	1.97	
	502	1.06	
	572	1.01	
	31	0.91	

[a] The internal coordinates are those of residue 8 in the middle of hexadecaglycine.
[b] The five largest amplitudes are listed except for localized NH stretch. The contribution to the total fluctuation from the five modes with the largest amplitudes varies from greater than 90% (NH stretch) to less than 30% ($NC^\alpha C'$ bend).

equal-time autocorrelations for each of the main-chain dihedral angles (ϕ,ψ, and ω) are shown in Fig. 4(a). Allowing for peptide-bond flexibility, the rms fluctuations in ϕ and ψ are 12°–13° in the middle of the helix, with greater fluctuations at the ends. Thus, unlike the bond length fluctuations, those in the dihedral angles are significantly reduced by the presence of structure and the resulting nonbonded contacts in the interior of the helix. In the study of $G\bar{o}$ and $G\bar{o}^{10}$ of an infinite helix in harmonic (ϕ,ψ) dihedral angle space, the rms fluctuations were significantly smaller ($\phi \sim 9°$, $\psi \sim 10.5°$). Increasing the rigidity of the helix by restricting twisting about ω (K_ω = 100 kcal/mol) significantly decreases the magnitude of the fluctuations in ϕ but has a much smaller effect on ψ [Fig. 4(a)]. This could be due to the fact that changes in the angle ϕ involve motions of the C=O group, which is more strongly coupled to heavy-atom displacements than is the NH group, which plays the corresponding role for ψ. Intermediate values of K_ω (7 kcal/mol) lead to intermediate results (Table IV). Removing the explicit hydrogen-bond potential results in only a small increase in the dihedral angle fluctuations. This is primarily a result of the fact that these fluctuations have only a small effect on the hydrogen-bond length

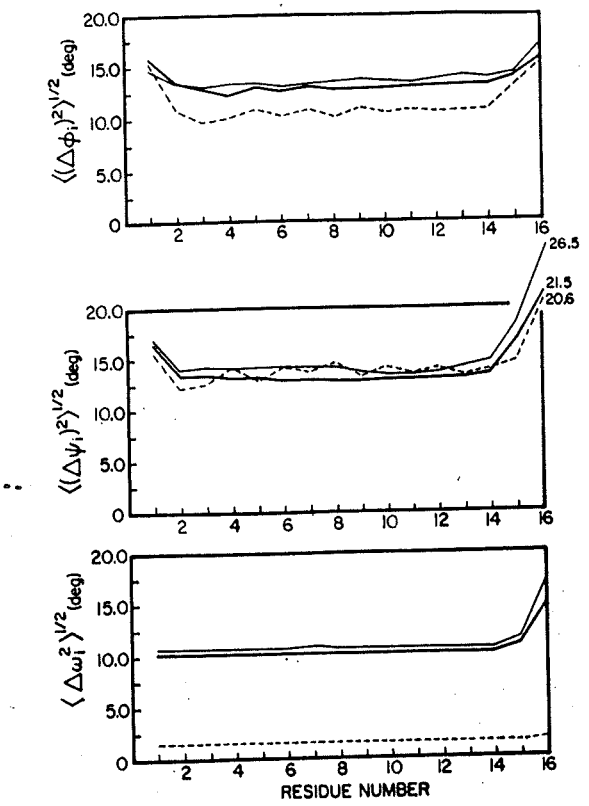

(a)

Fig. 4. Correlations of fluctuations of dihedral angles. (a) Equal-time autocorrelations of each of the dihedral angles in hexadecaglycine. (b) Normalized correlations in fluctuations of ϕ,ψ, and ω of residue 8 with the other dihedral angles of the helix. —, K_ω = 2.9 kcal/mol (flexible peptide bond); - - -, K_ω = 100 kcal/mol (rigid peptide bond); — no hydrogen bonds + flexible peptide bond.

(see below). The rms fluctuations in the improper dihedral angles, corresponding to motion of the amide hydrogen and carbonyl oxygen out of the plane of the peptide bond, are about 22° and 7.5°, respectively.

The spectral densities of representative dihedral angles and improper torsional angles are shown in Fig. 5. For the dihedral angles, a large number of low-frequency (<200 cm^{-1}) modes are seen to contribute; the dominant contributions came from 35–100 cm^{-1}. The improper N—H torsion is in a higher-frequency range (250–400 cm^{-1}, 500–600 cm^{-1}); the 500–600-cm^{-1} region, which makes a relatively small contribution, arises from coupling of the C=O and NH improper torsions.

Since the lowest frequency modes involve the most extensive displacements, there must be correlations among fluctuations of the dihedral angles

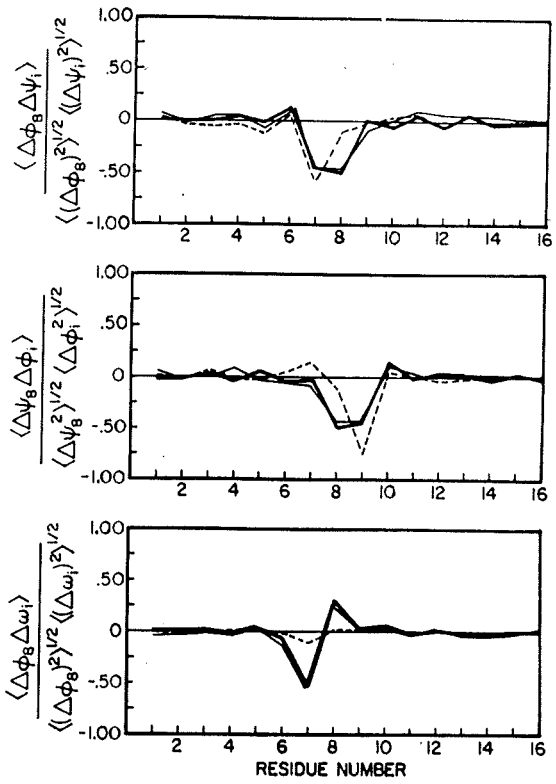

(b)

Fig. 4 (*continued from the previous page*)

if the secondary structure of the chain is to be maintained. Figure 4(b) shows the correlations in the fluctuations of ϕ and ψ of residue 8 in the middle of the 16-residue helix, within the same residue and with the dihedral angles in neighboring residues. Strong correlations exist between fluctuations of ϕ_8 and ψ_8 and between ϕ_8 and ψ_7, but the more distant correlations are damped out relatively quickly. Also, it is clear from the figure that ϕ_8 is strongly correlated with ω_8 and ω_7; the correlation between ψ_8 and ω_8 (not shown) is much weaker. The observed correlations are such as to localize the motion of the helix atoms. The strong anticorrelation of ϕ_8 and ψ_7 leads to oscillations of the peptide group between them ($[C{=}O]_7 - [NH]_8$) while keeping the rest of the helix fixed. Similarly, the ϕ_8 and ω_7 anticorrelation coupled with the ϕ_8,ω_8 correlation results in a localization of the helical distortion. The analysis of Gō and coworkers[10,11] of fluctuations in the dihedral angles of an α-helix showed observable correlations between dihedral angles as far as six residues apart, although the magnitudes beyond four are very small. In that work, only the ϕ and ψ dihedral angle were included. Apparently the additional flexibility inherent in a

TABLE IV
Fluctuations of Dihedral Angles Obtained with Different Peptide Bond Torsion Constants[a]

	$K_\omega = 2.9$	$K_\omega = 7.0$	$K_\omega = 100$
$\langle[\Delta\phi_6(0)]^2\rangle^{1/2}$	13.0	10.8	10.2
$\langle[\Delta\psi_6(0)]^2\rangle^{1/2}$	13.3	11.8	13.1
$\langle[\Delta\omega_6(0)]^2\rangle^{1/2}$	9.9	7.3	2.1
$\dfrac{\langle\phi_6(0)\Delta\psi_6(0)\rangle}{\langle\Delta\phi_6^2\rangle^{1/2}\langle\Delta\psi_6^2\rangle^{1/2}}$	−0.49	−0.41	−0.06
$\dfrac{\langle\Delta\phi_6(0)\Delta\psi_5(0)\rangle}{\langle\Delta\phi_6^2\rangle^{1/2}\langle\Delta\psi_5^2\rangle^{1/2}}$	−0.44	−0.49	−0.53

[a] Fluctuations in degrees; torsion constants in kcal/mol.

complete treatment that allows all degrees of freedom to vary leads to more rapid damping of the disturbances in helical structure induced by torsion-angle fluctuations. The present results are more similar to those obtained in a molecular dynamics study of bovine pancreatic trypsin inhibitor (PTI),[9] in which all degrees of freedom are included.

Restricting motion about the peptide dihedral angle has a strong effect on the correlation pattern. Gō and Gō,[10] who allowed only ϕ and ψ to vary, found that the correlations in the fluctuations of ϕ_i, ψ_i are small compared

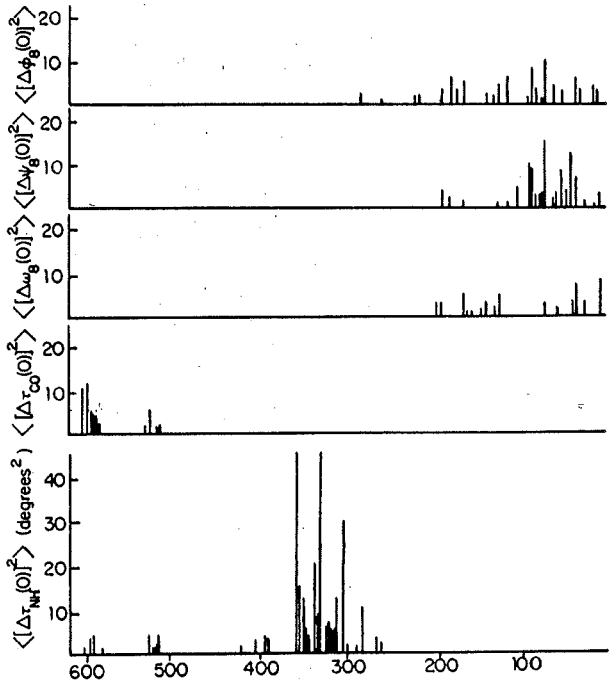

Fig. 5. Spectral densities of autocorrelations of dihedral angle (ϕ,ψ,ω) and improper torsion (τ_{NH},τ_{CO}) fluctuations. Modes contributing more than $(1°)^2$ to the total fluctuation are included.

to those of ϕ_i, ψ_{i-1}. Figure 4(b) shows that a similar result is obtained when motion about the peptide dihedral angle ω is completely restricted. Use of the intermediate value (K_ω = 7 kcal/mol) yields $\langle \Delta\phi_8 \Delta\psi_8 \rangle = -0.41$. This result is very similar to the one shown in Fig. 4(b) for K_ω = 2.9 kcal/mol and is also in close agreement with the values obtained in the α-helical part of PTI with K_ω = 7 kcal/mol; in the latter, the values of $\langle \Delta\phi_i, \Delta\psi_i \rangle$ averaged -0.40. It is of interest that for the β-sheet region of PTI, the correlations between distant residues were stronger and the $(\Delta\phi_i, \Delta\psi_i)$ correlation was found to be very small (see Fig. 4 of Ref. 9). A detailed study of β-sheet structure is planned to elucidate the differences between its dynamics and those of the α-helix.

The correlation patterns of the dihedral angles for the central residues of the 10-residue helix are the same as shown for the 16-residue helix in Fig. 4(b), indicating that the middle of the helix is not affected by the greater mobility of the ends. Correlations of fluctuations in ϕ_{16} with ψ_i and ω_i at the carboxyl terminal end of the helix, although qualitatively similar to the correlations in the middle of the helix, are different in the details of the observed pattern; e.g., $\langle \Delta\phi_{16} \Delta\psi_{16} \rangle$ is -0.25 as compared with -0.50 for the central residues, the correlations between $\Delta\phi_{16}$ and more distant residues are somewhat larger than found in the center of the helix.

Fluctuations of improper torsions of the carbonyl and amide groups that are hydrogen bonded to each other are not correlated. One reason for this is that the amide H torsional axis is rotated by almost 90° with respect to the carbonyl oxygen torsional axis, so that a simultaneous fluctuation of the same sign in both torsions is not as destructive of the hydrogen bond as if they were fluctuating about the same axis. Also, the spectral analysis of these motions indicates that they involve very different frequency ranges (see Fig. 5).

Figure 4(b) also shows the effect of removing the hydrogen-bond term in Eq. (1) on the correlation of dihedral-angle fluctuations. It is clear that the effect is almost negligible. This arises from the fact that the fluctuations under consideration lead to weak perturbation of the hydrogen bonds due to the flexibility of the system. By contrast, the presence of hydrogen bonds has a large effect on the overall length fluctuations of the helix (see below). An analysis of these striking differences is given in the section on potential energy surface calculations.

Length Fluctuations

The length fluctuations, which play an important role in the elastic properties of the helix, involve concerted motions of two or more residues. To determine their magnitude, the change in the projection of the center-of-mass coordinates of every residue onto the helix axis was obtained for each of the normal modes. The resultant length changes were then averaged over all the modes to obtain

$$\langle (\Delta l_{ij})^2 \rangle = \sum_\alpha \langle (\hat{n} \cdot [\mathbf{R}_{ij}^\alpha - \mathbf{R}_{ij}^0])^2 \rangle \tag{11}$$

where $\langle(\Delta l_{ij})^2\rangle$ is the fluctuation in the projected distance between residues i and j, $(\mathbf{R}_{ij}^{\alpha} - \mathbf{R}_{ij}^{0})$ is the fluctuation of the difference between the center-of-mass coordinates of residues i and j in the α normal mode, $\hat{n}$ is the unit vector in the direction of the helix axis, and the brackets represent the thermal average. Autocorrelations of fluctuations in the projected distance between adjacent residues (i and $i + 1$) of the helix in the presence and absence of hydrogen bonds are shown in Fig. 6. In contrast to the lack of effect of hydrogen bonds on dihedral-angle correlations, the presence of hydrogen bonds significantly suppresses length fluctuations. An examination of the frequency spectrum of length fluctuations (Table V) and a comparison with the spectra of dihedral angle correlations (Fig. 5) is helpful for the interpretation of this result. Most of the vibrational modes of the helix, including those involved in dihedral angle fluctuations, are length preserving due to the correlation involved. Essentially only the lowest frequency modes (<25 cm^{-1}) contribute to length fluctuations. It can be seen from the table that it is just these low-frequency modes that have a large fractional reduction in frequency and correspondingly increase in amplitude when the hydrogen bonds are excluded. For the modes that contribute to the dihedral angle fluctuation (35–150 cm^{-1} in the complete potential), the fractional change in frequency is much smaller (on the order of 0.1) on deleting the hydrogen bonds.

Fluctuations in length as a function of initial length are shown in Fig. 7, and the contributing normal modes are given in Table V. Each point represents an average over the appropriate portions of the helix; e.g., the fluctuations in the length of a segment three residues long was obtained by averaging over fluctuations in the length between residues 1 and 3, 2 and 4, 3 and 5, etc. When hydrogen bonds are excluded from the potential energy function, the length fluctuations are dramatically increased; the mean-square fluctuation in length of a segment is two to five times greater than in the presence of hydrogen bonds. This is a manifestation of the same behavior as observed for the nearest-neighbor projected distance

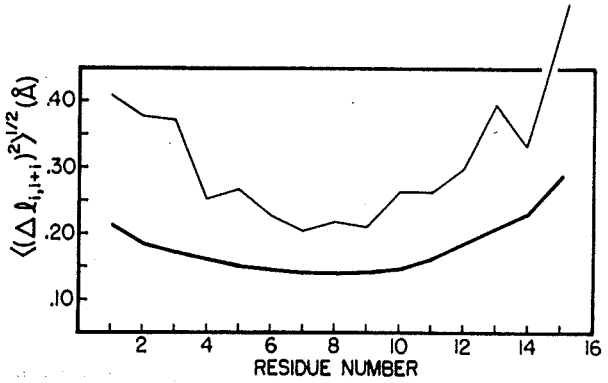

Fig. 6. Fluctuations in length between adjacent residues (residue i and $i + 1$): hydrogen bonds included in the potential (—); hydrogen bonds excluded from the potential (—).

TABLE V
Spectral Densities of Length Fluctuations for the Five Lowest Frequency Modes

Frequency (cm^{-1})	$\langle[\Delta l(2,16)]^2\rangle$[a] ($Å^2 \times 10^2$)
A. Hydrogen Bonds Included in the Potential	
7.81	1.21
13.41	0.12
14.70	2.83
17.90	0.06
23.23	0.06
Sum over all frequencies	7.38
B. Hydrogen Bonds Excluded from the Potential	
6.16	4.50
7.11	10.83
8.21	3.61
14.14	8.17
15.97	0.79
Sum over all frequencies	39.27

[a] Square of the length fluctuation between the second and last residues.

fluctuation. Although the length fluctuation generally increases with segment length as expected, the observed result is not monotonic. In particular, there is a reduction in the fluctuation when the first intrasegment hydrogen bond forms (6 Å) and at multiples of this distance.

From the large standard deviation given in Fig. 7, it is apparent that length fluctuations are very sensitive to position in the helix. For small α-helical fragments, segmental motion is strongly influenced by proximity to the ends of the helix, where there is greater mobility (see Fig. 6). Several authors[11,17,18] have used normal coordinate methods adapted for infinite

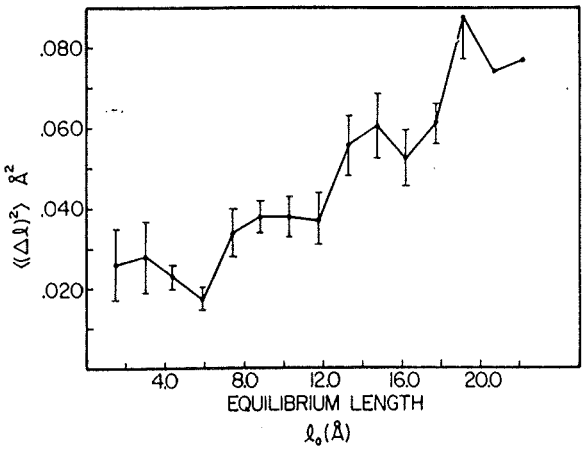

Fig. 7. Fluctuations in length within hexadecaglycine as a function of equilibrium length; each point is obtained by averaging over equal-sized segments of the helix (see text).

systems to study the dynamics expected for segments buried within very long helices. Calculations reported in the literature are compared with the present results in Table VI. It can be seen that for helices of the same length including hydrogen bonds, the values are very similar. Also, it is shown that the rms fluctuation is more than twice as large when the hydrogen-bond terms are removed. Related results have been obtained by Fanconi and Peticolas,[17] who used a simplified representation of an infinite helix.

Fanconi and Peticolas[17] and Itoh and Shimanouchi[16] have constructed frequency versus phase angle dispersion curves for several dynamical models of the helix and compared the curves obtained in the presence and absence of hydrogen bonds. Of particular interest in the work of Fanconi and Peticolas[17] is the separation that occurs between the longitudinal (stretch) and transverse (bend and twist) acoustical modes for a 16-residue helix as the hydrogen-bond force constant is varied from 0 to 0.30 mdyn/Å; the transverse mode is of lowest frequency. The lowest frequency modes obtained for our normal-mode treatment of the 16-residue helix do not show clear separation between stretching and torsional motion; in fact, the lowest frequency mode is largely a stretch. The lack of symmetry inherent in a treatment of a small, finite α-helix mixes the low-frequency modes, so that a distinct completely symmetric stretch is not observed. Another consequence of the end effects is that the elastic modulus is strongly length dependent for short helices. For the present system, the elastic modulus varied from 2.7×10^{11} dyn/cm^2 for a 4-peptide helix (one turn) to 2.3×10^{11} dyn/cm^2 for the 16-peptide helix. The latter result, obtained in the harmonic approximation is to be compared with the values ($1.7–4.8 \times 10^{11}$ dyn/cm^2) given above.

Fluctuations in length were also extracted from a vibrational analysis with ω held rigid. Length fluctuations for different portions of the helix when ω was rigid showed an even greater variation than the results of Fig. 7, because increasing the rigidity of the molecule exaggerates the end effects.

TABLE VI

Root-Mean-Square Displacements of the End-to-End Length Obtained by Different Authors

Source	Number of Residues	$\langle(\Delta l)^2\rangle^{1/2}$ (Å)	
		Gly α-Helix	Ala α-Helix
Suezaki and Gō (Ref. 11)	15	0.29	0.23
	18	0.31	0.24
Peticolas (Ref. 18)	10.8[a]		0.21
	18		0.38
Present work	15	0.28	
	15	(0.63)[b]	

[a] Number of peptide groups.

[b] Hydrogen bonds excluded from the potential.

Potential Energy Surfaces

To analyze the fluctuations and correlations described above, we examine the potential energy surface governing the (ϕ,ψ) torsional angles. Since it is not possible to visualize the multidimensional energy surface of a finite helix, we have examined slices through the full surface; in particular, we consider the two-dimensional surface for the central angles (ϕ_6,ψ_6) of decaglycine in various approximations. The rigid total-energy contour map given in Fig. 8 (upper-left map) represents the surface that would determine the motion of the helix if all the bond lengths, angles, and dihedral angles except ϕ_6 and ψ_6 were fixed rigidly at their equilibrium values. The contours are approximately elliptical close to the minimum; the orientation of the ellipses is such as to imply a large negative correlation between fluctuations of ϕ_6 and ψ_6, in accord with the results given above. The rigid total energy surface is determined primarily by the hydrogen-bond term for the angular range of interest (Fig. 9). The nonbonded contribution only becomes important for larger angles, while the electrostatic interaction shifts the low-energy region somewhat in the $(-\phi,-\psi)$ quadrant.

The rigid-surface results disagree with the vibrational analysis (see above), which demonstrated that for fluctuations in ϕ_i and ψ_i the presence of hydrogen bonds has a minor effect. Because there are many correlations among the various degrees of freedom, the two-dimensional rigid contour maps do not adequately represent the structural features of the energy surface that determine the fluctuations. A more adequate representation can be obtained from the total adiabatic energy surface shown in Fig. 8 (upper right); it gives the total potential energy as a function of ϕ_6 and ψ_6, with simultaneous relaxation of the other degrees of freedom. It is evident that the adiabatic map is much less restrictive. The most important difference between the rigid and flexible surface is due to the hydrogen-bond term. It was dominant for the rigid surface but is negligible over the range considered for the adiabatic potential (Fig. 9). Clearly the adjustment of atom positions in the latter calculation permits the hydrogen bonds to remain essentially unchanged while the torsional angles are varied over a significant range. To confirm this result we give in Table VII the values of parameters associated with the helix hydrogen bonds in the adiabatic calculation for two extreme pairs of torsional angles; that is, we compare the adiabatic results for $\Delta\phi = -20°$, $\Delta\psi = -20°$ and $\Delta\phi = +20°$, $\Delta\psi = -20°$ with those for the equilibrium geometry. It is evident from the table that all of the O···H hydrogen-bond lengths remain close to their optimum values. There are significant changes in the bond angles involved for O_2···H_6 through O_5···H_9, but the adjustments in geometry are sufficient to yield an essentially constant value for the total hydrogen-bond energy. Listed in Table VIII are the changes that occur in the dihedral angles. It is apparent that energy minimization leads to more extensive alterations throughout the helix when ϕ and ψ are rotated in the same direction as compared with rotations of opposite sign. For $\Delta\phi_6 = -20°$, $\Delta\psi_6 = -20°$ changes in the dihedral angles occur in all residues except the first; for $\Delta\phi_6 = +20°$, $\Delta\psi_6$

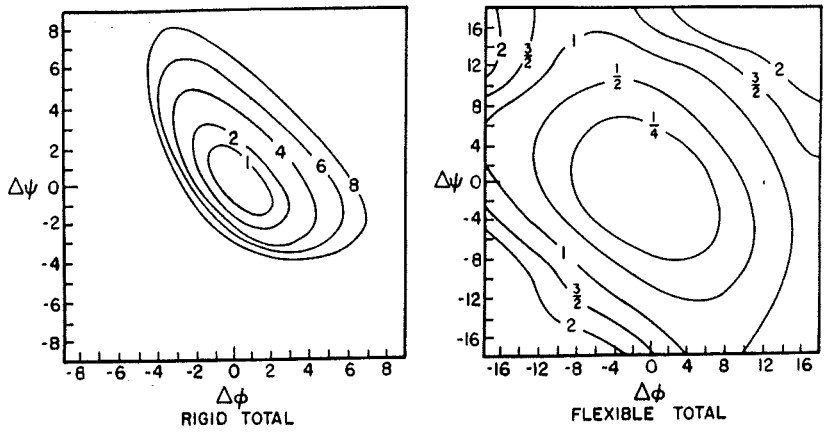

(a)

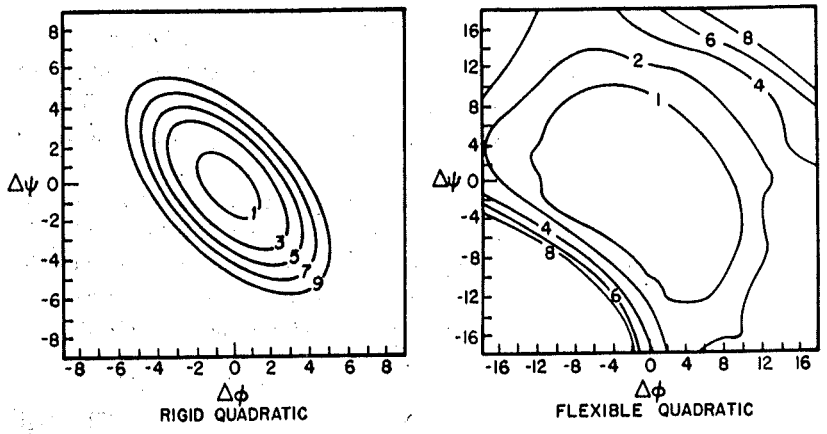

(b)

Fig. 8. Two-dimensional potential energy surface for the central angles (ψ_6, ψ_6) of decaglycine in the different approximations. Upper left, rigid total energy surface; upper right, flexible total energy surface. Lower left and right, are respectively, the rigid quadratic energy and flexible quadratic energy surfaces. Contour units are in kcal/mol.

$= -20°$ the changes are more restricted. It should be noted that the peptide dihedral angles of residues 5 and 6 are increased by more than 10°; this would be somewhat reduced if K_ω were higher.

The dihedral angle dependence of the energy contributions to the adiabatic surface (Fig. 8) can be divided approximately into two regions with respect to a diagonal line that extends from ($\Delta\phi = -20°$, $\Delta\psi = +20°$) to ($\Delta\phi = +20°$, $\Delta\psi = -20°$). Above the diagonal, increases in the torsional energy make the major contribution, while below the diagonal the surface

TABLE VII
Changes from Equilibrium Values for Two Conformations on the Flexible Surface[a]

Residue	$\Delta\phi$	$\Delta\psi$	$\Delta\omega$	$\Delta\phi$	$\Delta\psi$	$\Delta\omega$
1	—	—	—	—	—	—
2	−4.50	—	−3.64	—	—	—
3	—	+5.52	−4.81	—	—	—
4	—	−8.40	+5.50	—	—	—
5	+2.08	−12.05	+12.50	—	−7.30	−7.91
6	(−20)[b]	(−20)[b]	+10.10	(+20)[b]	(−20)[b]	+13.10
7	−4.65	—	+3.99	−3.35	−7.20	+4.83
8	−13.65	+10.21	−6.37	−2.88	+4.09	+2.48
9	+4.23	—	−4.86	−2.93	—	−3.50
10	—	−5.90	—	—	−4.05	—

[a] Angles in degrees.
[b] Constrained angles.

depends on both the nonbonded and electrostatic energy contributions. For neither region is the hydrogen-bond energy important.

A very important question concerns the validity of the harmonic approximation to the dynamics of an α-helix, in particular, and of polypeptides and proteins, in general. Skvortsov et al.[37] used a Monte Carlo method to study the dihedral angle fluctuation of α-helices. The empirical potential employed consisted only of a hydrogen-bond potential expressed as a function of a dihedral angle ϕ,ψ; with this potential function, the mean energy per residue in the harmonic approximation is $\langle(E - E_{\min})\rangle = KT$. They found the mean energy per residue was $0.8KT$ with a Lippencott-Schroeder hydrogen-bond potential and $0.6KT$ with a Morse potential.

To examine the importance of anharmonic contributions to the potential function used in the present work, we have constructed the quadratic ap-

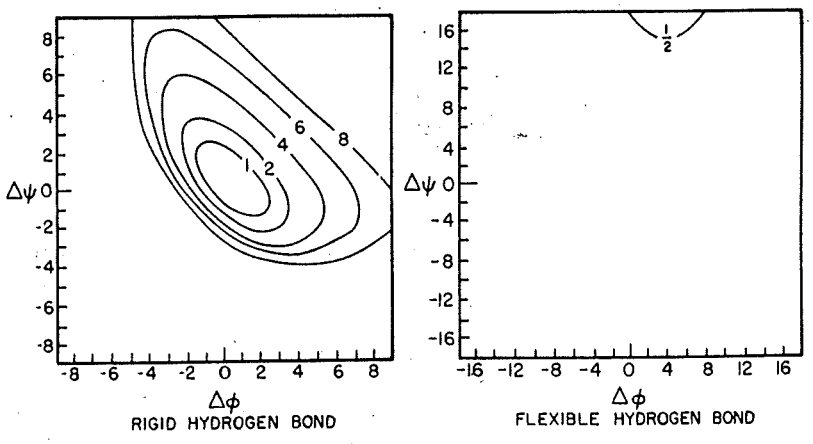

Fig. 9. Hydrogen-bond contribution to the rigid total potential energy surface (left) and to the flexible total potential surface (right).

TABLE VIII
Hydrogen-Bond Parameters at Two Points on the Adiabatic Flexible Surface of Decaglycine[a]

H Bond	Equilibrium Geometry			$\Delta\phi = -20°, \Delta\psi = -20°$			$\Delta\phi = +20°, \Delta\psi = -20°$		
	R_{O-H}	θ_{N-H-O}	θ_{H-O-C}	R_{O-H}	θ_{N-H-O}	θ_{H-O-C}	R_{O-H}	θ_{N-H-O}	θ_{H-OC}
O (terminal)···H_4	1.89	164	151	1.88	161	169	1.89	166	150
O_1···H_5	1.89	163	164	1.89	154	160	1.89	163	165
O_2···H_6	1.89	163	166	1.91	164	105	1.89	157	163
O_3···H_7	1.89	162	163	1.91	132	95	1.89	161	145
O_4···H_8	1.89	162	165	1.89	128	114	1.89	167	145
O_5···H_9	1.89	161	163	1.89	144	165	1.89	159	135
O_6···H_{10}	1.89	161	163	1.89	159	163	1.89	166	163
O_7···H (terminal)	1.89	149	161	1.89	149	143	1.89	154	166
Total energy	−30.9 kcal/mol			−30.9 kcal/mol			−30.9 kcal/mol		

[a] Distances in Å and angles in degrees.

TABLE IX
Fluctuations Obtained from Potential Surfaces

Potential Surface	$\langle \Delta\phi_6^2 \rangle^{1/2}$	$\langle \Delta\psi_6^2 \rangle^{1/2}$	$\frac{\langle \Delta\phi_6 \Delta\psi_6 \rangle}{\langle \Delta\phi_6^2 \rangle^{1/2} \langle \Delta\psi_6^2 \rangle^{1/2}}$
Rigid total	1.53	1.44	−0.57
Rigid quadratic	1.34	1.37	−0.64
Adiabatic total	9.14	9.31	−0.24
Adiabatic quadratic	7.06	7.27	−0.40
Vibrational result	12.69	12.89	−0.46

proximations to the rigid and adiabatic *total* energy surfaces for (ϕ_6,ψ_6) by the method described above. The rigid quadratic potential (Fig. 8) averages the asymmetric effects of the hydrogen and nonbonded terms, and the result is a set of concentric ellipses about the equilibrium geometry. The adiabatic quadratic surface is more complicated, but it still has a high degree of symmetry even though the geometry is determined by the interaction of nonbonded, electrostatic, and torsional effects. Comparing the total surfaces to the quadratic approximations indicates that differences exist but that they are not large.

Additional information is provided by the fluctuations in ϕ_6 and ψ_6 estimated from the four potential surfaces by Eq. (9); the results are presented in Table IX. The quadratic surfaces are more restrictive than the corresponding total energy surfaces, and there is a higher correlation between fluctuations when the averages are obtained with the quadratic surfaces. It is clear from Fig. 8 and Table IX that the rigid potential surface is not adequate for simulating molecular dynamics. The averages obtained with the adiabatic quadratic surface resemble the vibrational results more closely. Summing over a larger portion of the adiabatic surface ($|\phi|, |\psi| > 20°$) would increase the magnitude of the calculated fluctuations and bring them into closer agreement with the harmonic dynamic values.

It is more difficult to evaluate the importance of the discrepancies between the results for the adiabatic total surface and those obtained with the quadratic approximation. There is some suggestion that the anharmonic contributions are significant. For both ϕ and ψ, Table IX shows that the expected rms fluctuation is greater in the adiabatic total map than it is in the adiabatic quadratic map. This difference, which is due to anharmonicity contributions, would be accentuated if the summation were extended to include the complete conformational space available at room temperature; comparison of the vibrational result with the adiabatic quadratic value provides an indication of the magnitude of the expected difference. To obtain the exact value of the importance of anharmonic effects, it would be necessary to compare the harmonic dynamics with a full molecular dynamics treatment of the helix.

Time Dependence of Fluctuations

In addition to the magnitudes and correlations of fluctuations, their time dependence is of considerable interest. By use of the methods described above, the normalized position and velocity time correlation functions for the internal coordinates were evaluated in the harmonic approximation. The position results obtained for the central dihedral and improper torsional angles of the 16-residue helix are shown in Fig. 10, and the velocity results for ϕ and ψ are given in Fig. 11. The bond lengths and bond angles are not given, because their decay behavior is of less interest than the softer dihedral angles.[9] From Fig. 10 it is evident that the three dihedral angles (ϕ_8, ψ_8, ω_8) all show a rapid decay ($\sim$0.1 psec) with a negative excursion and subsequent smaller oscillations. Their appearance is that expected from an underdamped torsional oscillator in that they undergo several periods of vibration of successively decreased amplitude. The improper torsions are very different in that there are well-defined periodic oscillations with a slow decay superimposed on them; in particular, the C=O improper torsion exhibits a beating phenomenon expected from the superposition of a small number of harmonic frequencies—one with a period of $\sim$0.1 psec and the other with a period of $\sim$0.5 psec. An analysis of the power spectrum of these correlation functions (Fig. 5) reveals that the five largest contributing frequencies account for 70% of the fluctuations in the carbonyl oxygen torsion, 45% of the amide hydrogen torsion, and about 25% of the fluctuations in the backbone dihedral angles ϕ and ψ. The velocity correlation functions appear more harmonic than the position correlation, because the former are more sensitive to the high-frequency end of the vibrational spectrum [Eq. (5)], which consists of a few well-separated peaks in contrast to the broad bands in the low-frequency portion.

In the general analysis of molecular motion, it is possible to identify two extreme mechanisms which can contribute to the time decay in the autocorrelation function. One of these is referred to as "dephasing" and the other as "energy dissipation."[38] If one focuses attention on the motion of a small group of atoms within a macromolecule, these atoms will be observed to move in a stochastic manner due to thermal interaction with many other degrees of freedom of the system.[38] Starting with a normal mode analysis, the effect of the interactions due to anharmonic terms is to allow energy transfer from one mode to another. The Langevin equation can provide a phenomenological description of the dynamics of such an energy dissipation process. For a completely harmonic system, energy dissipation is excluded, since all the dynamical variables are periodic functions of time. For a local motion (e.g., a dihedral angle) that does not correspond to a normal mode, loss of correlation can nevertheless occur. This is attributable to dephasing of the normal coordinate components of that motion and can also be treated in terms of a Langevin equation.[39,40] Whether dephasing is observed for a particular coordinate depends on the details of the frequency spectrum; i.e., a large number of closely spaced peaks will result in dephasing. It is this type of decay in the correlation function that

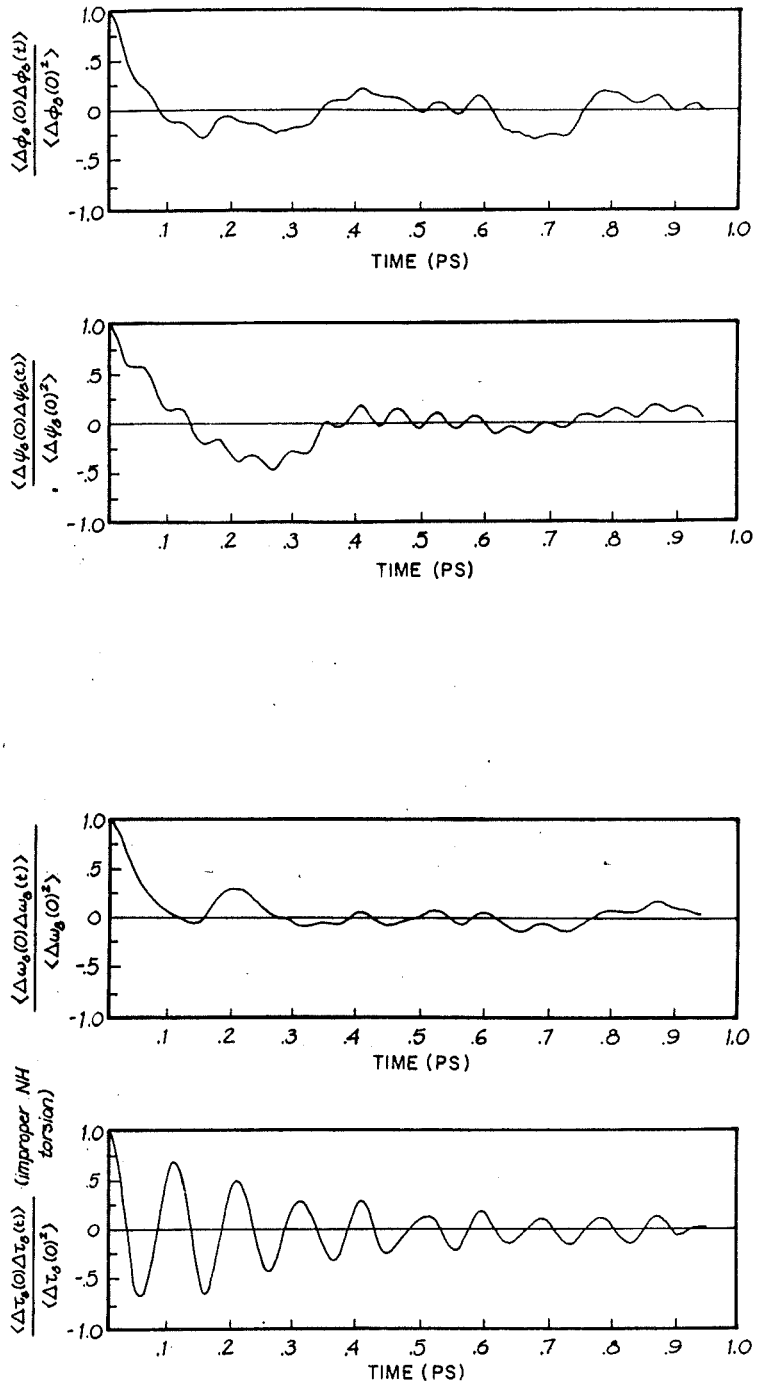

Fig. 10. Normalized time correlations of internal coordinate positions for the central dihedral and improper torsional angles of the 16-residue helix.

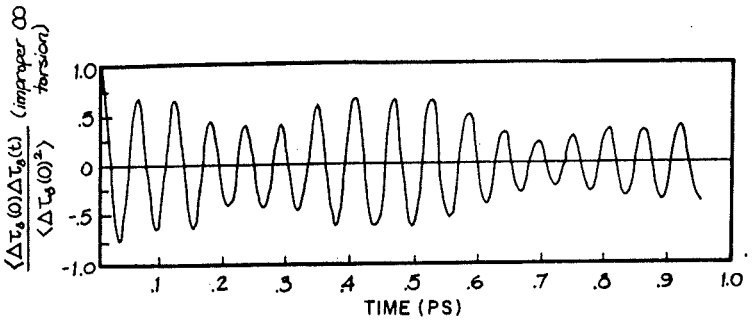

Fig. 10 (*continued from the previous page*)

is shown in Fig. 10 for the harmonic approximation to the α-helix. Ultimately, due to constructive interference of the contributing normal modes, the correlation function must increase in magnitude again; however, this periodic behavior has not been examined except for the C=O improper torsion.

Both dephasing and energy dissipation processes have been studied in an attempt to interpret the bandwidths of Raman lines in the vibrational spectroscopy of liquids.[41] Dephasing in liquids has been shown to be an efficient relaxation mechanism, as it is for the harmonic model of the α-helix. The relative contribution of dephasing and energy dissipation

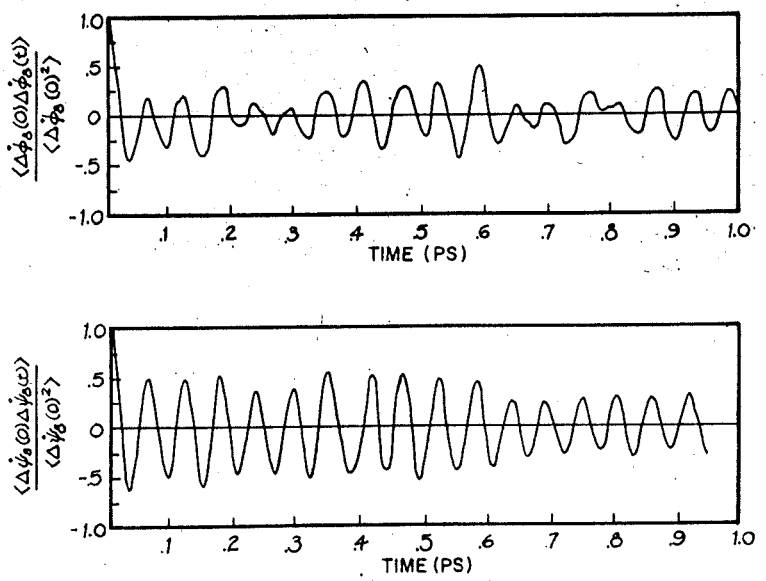

Fig. 11. Normalized time correlations of internal coordinate velocities for the central dihedral angles ϕ and ψ of the 16-residue helix.

in the decay of time correlation functions of polypeptide and protein coordinates remains to be investigated.

We thank Dr. J. A. McCammon for helpful discussions and Prof. W. Peticolas for comments on the manuscript. Many of the programs used for this work were developed by Dr. B. R. Gelin. Dr. Paul Weiner kindly provided the conjugate gradient minimization routine. This work was supported in part by the National Institutes of Health, and in part by a Fellowship to R. M. L. from the American Heart Association.

References

1. Campbell, I. D., Dobson, C. M., Moore, G. R., Perkins, S. J. & Williams, R. J. P. (1976) *FEBS Lett.* **70**, 96–98.
2. Dobson, C. M. (1977) in *NMR in Biology*, Dwek, R. A., et al., Eds., Academic, London, p. 63.
3. Oldfield, E., Norton, R. A. & Allerhand, S. J. (1975) *J. Biol. Chem.* **250**, 6368–6379.
4. Allerhand, A. & Komoroski, R. A. (1973) *J. Am. Chem. Soc.* **95**, 8228–8231.
5. Fossel, E., Veatch, W. R., Ovchinnikov, Y. A. & Blout, E. R. (1974) *Biochemistry* 13, 5264–5272.
6. Lipscomb, W. N. (1970) *Acc. Chem. Res.* **3**, 81–89.
7. Torchia, D. A. & Lyerla, J. R. (1974) *Biopolymers* **13**, 97–114.
8. Torchia, D. A. & Lyerla, J. R. (1974) in *Peptides, Polypeptides and Proteins, Proceedings of the Rehovot Symposium on Poly-Amino Acids*, Blout, E. R. et al., Ed., Wiley, New York, pp. 436–448.
9. McCammon, J. A., Gelin, B. R. & Karplus, M. (1977) *Nature* **267**, 585–590.
10. Gō, M. & Gō, N. (1976) *Biopolymers* **15**, 1119–1127.
11. Suezaki, Y. & Gō, N. (1976) *Biopolymers* **15**, 2137–2153.
12. Gelin, B. R. & Karplus, M. (1977) *Proc. Natl. Acad. Sci. USA* **74**, 801–805.
13. McCammon, J. A. & Karplus, M. (1977) *Nature* **268**, 765–766.
14. Fanconi, B., Small, E. & Peticolas, W. L. (1971) *Biopolymers* **10**, 1277–1298.
15. Miyazawa, T., Fukushima, K., Sugano, S. & Masuda, Y. (1967) in *Conformations of Biopolymers*, Ramachandran, G. N., Ed., Academic, London, pp. 557–568.
16. Itoh, K. & Schimanouchi, T. (1970) *Biopolymers* **9**, 383–399.
17. Fanconi, B. & Peticolas, W. (1971) *Biopolymers* **10**, 2223–2229.
18. Peticolas, W. (1978) *Methods Enzymol.* **61**, 425–458.
19. Brown, K. G., Erforth, S. C., Small, E. W. & Peticolas, W. L. (1972) *Proc. Natl. Acad. Sci. USA* **69**, 1467–1469.
20. Gelin, B. R. & Karplus, M. (1975) *Proc. Natl. Acad. USA* **72**, 2002–2006.
21. Gelin, B. R. & Karplus, M. (1979) *Biochemistry* **18**, 1256–1268.
22. Hagler, A. T. & Lifson, S. (1974) in *Peptides, Polypeptides and Proteins*, Blout, E. R. et al., Ed., Wiley, New York, pp. 35–47.
23. Dodson, E. J., Issacs, N. W. & Rollett (1976) *Acta Crystallogr., Sect. A* **32**, 311–315.
24. Ralston, A. & Wilf, H., Eds. (1966) *Mathematical Methods for Digital Computers*, Wiley, New York.
25. Wilson, E. B., Decius, J. C. & Cross, P. C. (1955) *Molecular Vibrations*, McGraw-Hill, New York.
26. Zwanzig, R. A. (1965) *Ann. Rev. Phys. Chem.* 16, 67–102.
27. Wang, M. C. & Uhlenbeck, G. E. (1945) *Rev. Mod. Phys.* **17**, 323–342.
28. Heer, C. V. (1972) *Statistical Mechanics, Kinetic Theory and Stochastic Processes*, Academic, New York.
29. IUPAC-IUB Commission on Biochemical Nomenclature (1970) *Biochemistry* **9**, 3471–3478.
30. Gō, N., Gō, N. & Scheraga, H. (1970) *J. Chem. Phys.* **52**, 2060–2079.
31. Shimanouchi, T., Asahina, M. & Enomoto, S. (1962) *J. Polym. Sci.* **59**, 93–100.
32. Feughelman, M. & Druhala, M. (1977) *J. Polym. Sci.* 15, 311–314.

33. Kotoda, S., Takagi, K., Vematsu, V. & Vematsu, I. (1972) *Rep. Prog. Polym. Phys. Jpn.* 15, 629–632.
34. Harley, R., James, D., Miller, A. & White, J. (1977) *Nature* 267, 285–287.
35. Suzuki, S., Iwashita, Y., Shimanouchi, T. & Tsuboi, M. (1966) *Biopolymers* 4, 337–350.
36. Rabott, J. F., Moore, W. H. & Krimn, S. (1977) *Macromolecules* 10, 1065–1074.
37. Skvortsov, A. M., Birshtem, T. M. & Aleksanyan, V. I. (1972) *Mol. Biol.* 6, 491–497.
38. McCammon, J. A., Wolynes, P. G. & Karplus, M. (1979) *Biochemistry* (in press).
39. Maradudin, A. A., Montroll, E. W., Weiss, G. H. & Ipatova, I. P. (1971) *Theory of Lattice Dynamics in the Harmonic Approximation*, 2nd ed., Academic, New York.
40. Adelman, S. A. & Garrison, B. J. (1976) *J. Chem. Phys.* **65**, 3751–3761.
41. Fischer, S. & Laubereau, A. (1975) *Chem. Phys. Lett.* 35, 6–8.

Received October 30, 1978
Accepted March 30, 1979